ORIGINAL ARTICLE

In situ growth of redox-active iron-centered nanoparticles on graphene sheets for specific capacitance enhancement

Puteri Emme Marina [a,1], **Gomaa A.M. Ali** [a,b,1], **Li Min See** [a], **Ellie Yi Lih Teo** [a], **Eng-Poh Ng** [c], **Kwok Feng Chong** [a,*]

[a] *Faculty of Industrial Sciences & Technology, Universiti Malaysia Pahang, Gambang, 26300 Kuantan, Malaysia*
[b] *Chemistry Department, Faculty of Science, Al-Azhar University, Assiut 71524, Egypt*
[c] *School of Chemical Engineering, Universiti Sains Malaysia, Engineering Campus, 14300 Nibong Tebal, Pulau Pinang, Malaysia*

Abstract   A fast and facile approach is proposed to enhance the specific capacitance of N-Methyl-2-pyrrolidone (NMP)-exfoliated graphene. Redox-active nickel ferricyanide (NiFeCN) nanoparticles were grown on the surface of graphene sheets using a simple co-precipitation method. Apart from the synergetic effect of graphene as double layer capacitance and NiFeCN as pseudocapacitance in specific capacitance enhancement, the NiFeCN nanoparticles served as the spacer to prevent the graphene sheets agglomeration. The NiFeCN/graphene exhibited specific capacitance of 113.5 F g^{-1}, which was 2 times higher than the NMP-exfoliated graphene (52 F g^{-1}) and 6 times higher than the pure NiFeCN (18 F g^{-1}). The findings suggested the NiFeCN/graphene could be the potential candidate for supercapacitor electrode.

1. Introduction

Supercapacitors are the energy storage devices that provide higher energy density than the conventional capacitors and are able to deliver them at a faster rate than batteries. The charge storage mechanisms in supercapacitors can be classified into electrochemical double layer capacitance (EDLC) and pseudocapacitance. The former stores energy in the form of ions adsorption on the electrode surface, while in the latter, the capacitance originates from the redox reaction at the active sites of the electrode materials. The common materials with EDLC properties are the carbon-based materials such as activated carbon, carbon nanotube, graphene, carbon onion and fullerene (Ali et al., 2015, 2014b; Borgohain et al., 2014; Cao et al., 2014;

* Corresponding author. Tel.: + 60 9 5492403; Fax: + 60 9 5492766.
  E-mail address: ckfeng@ump.edu.my (K.F. Chong).
[1] P.E. Marina and G.A.M. Ali contributed equally to this work as first authors.

Krishnamoorthy et al., 2015; Liu et al., 2010, 2014; Teo et al., 2015; Zaid et al., 2015; Zhang et al., 2015). On the other hand, metal oxides (RuO_2, MnO_2, NiO, Co_3O_4) and conducting polymers (polyaniline, polypyrrole), which could have faradaic reaction in the electrolyte system, possess significant pseudocapacitance effect (Ali et al., 2014a,c; Arslan and Hür, 2012; Pang et al., 2015a,b; Ramya et al., 2013; Vidhyadharan et al., 2014; Wang et al., 2013; Wu et al., 2010). Often, EDLC and pseudocapacitance materials are applied collaboratively in hybrid supercapacitors in order to deliver higher energy output with better stability.

Graphene, a unique two-dimensional carbon material was proposed as an excellent electrode material in replacing activated carbon as the incumbent in supercapacitors, due to its good conductivity, chemical inertness, excellent mechanical properties and high specific surface area (Ali et al., 2015; Chen et al., 2015; Liu et al., 2010; Teo et al., 2012, 2015; Wang et al., 2009). The intrinsic capacitance of graphene was reported to be 21 mF cm^{-2}, the highest value among all carbon-based materials (Liu et al., 2015). High quality and low defects graphene sheets could be produced *via* chemical vapor deposition and epitaxial growth technique (Gao et al., 2010; Liu et al., 2011). However, scale-up production for these surface-based techniques remains challenge when large quantities of graphene are needed. Chemical modified graphene or reduced graphene oxide *via* Hummers' method has been introduced for large scale production of graphene (Krishnamoorthy and Kim, 2015; Sun and Fugetsu, 2013). Again, strong reductants such as hydrazine used in this technique would cause environmental issue for its disposal. The quest for mass production of graphene never stops, and the new method by ultrasonicating graphite in NMP solvent was reported in 2008 (Hernandez et al., 2008). This approach is a promising protocol as high quality and unoxidized graphene could be produced and 12 wt% of monolayer graphene could be achieved. Despite its high yield production, the applicability of NMP-exfoliated graphene in supercapacitor is still limited, probably due to the severe sheets agglomeration problem upon solvent removal. Therefore, it is of great importance of having graphene sheets that are separated within the electrode in order to enhance the electrochemical performance of the supercapacitors. Previous study reported that tosyl functional groups were first introduced and decorated on the defect sites of graphene, prior to NMP exfoliation process. Tosylate graphene showed good dispersibility with insignificant sheets aggregation and exhibited excellent specific capacitance of 180 F g^{-1} (Wen et al., 2014). To the best of our knowledge, there is no other reported work on the modification of NMP-exfoliated graphene for supercapacitor applications.

In this work, a facile co-precipitation approach was used to grow the redox-active nickel ferricyanide (NiFeCN) nanoparticles on the NMP-exfoliated graphene sheets. The NiFeCN should serve as the spacers to prevent the agglomeration of graphene sheets in the composite. Besides, the electrochemical properties of this composite should combine the benefits of the pseudocapacitance arising from the inclusion of NiFeCN and the EDLC formed at the surface of the graphene. The electrochemical performance of NiFeCN/graphene was evaluated by cyclic voltammetry, galvanostatic charge discharge and impedance spectroscopy.

2. Experimental section

Graphite powder (extra pure) was purchased from Merck. Nickel(II) nitrate hexahydrate ($Ni(NO_3)_2 \cdot 6H_2O$), potassium ferricyanide ($K_3Fe(CN)_6$), potassium nitrate (KNO_3), *N*-methyl-2-pyrrolidone (C_5H_9NO) and ethanol (C_2H_5OH) were purchased from Sigma–Aldrich. All reagents in this work were of analytical grade and used without further purification.

Graphene sheets were prepared by liquid phase exfoliation of graphite. The graphite powder was first dispersed in NMP at a concentration of 10 mg mL^{-1} and then sonicated for

1 h. The unexfoliated graphite platelets were removed by centrifuging the suspension for 90 min at 500 rpm. Graphene sheets were recovered from the supernatant by vacuum filtration through a 100 nm polyvinylidene fluoride (PVDF) membrane before drying under vacuum at room temperature. The yield of graphene sheets was about 28 wt% of the graphite powder used in this work. This method was proven to produce graphene platelets (Hernandez et al., 2008). However, graphene sheets tend to agglomerate upon solvent removal and hence, co-precipitation method was used to grow NiFeCN nanoparticles on graphene sheets, as illustrated in Scheme 1. In general, graphene sheets (3.33 g) were first dispersed and sonicated in a mixed solvent of ethanol and water (500 mL), which lead to the release of stacked graphene sheets to give well-separated individual sheets. With stirring, $Ni(NO_3)_2$ (500 mL, 0.1 M) was then added into the graphene dispersion before adding in $K_3Fe(CN)_6$ (500 mL, 0.1 M). The stirring was continued for 30 min at room temperature. The mixture was filtered, washed and dried at 80 °C for 8 h. The sample was then denoted as NiFeCN/graphene. NiFeCN/graphene samples with different Fe loadings were prepared by using different amounts of $K_3Fe(CN)_6$.

The structure and morphology of NiFeCN/graphene were investigated by X-ray diffraction (XRD, Rigaku MiniFlex II), Fourier transform infrared spectroscopy (FTIR, Perkin Elmer Spectrum 100) and field emission scanning electron microscope (FESEM, JEOL JSM-7800F). The transmission electron microscopy (TEM) analysis was performed using a Philips CM12 microscope with acceleration voltage of 200 kV. The electrochemical performance of NiFeCN/graphene samples were evaluated by cyclic voltammetry, galvanostatic charge/discharge and impedance spectroscopy in 3-electrode system. The working electrode was prepared by coating homogenous mixture (sample, carbon black and PTFE at the ratio of 90:5:5 in ethanol) onto a nickel foam. The active mass loading of the working electrode was approximately 4 mg. Platinum wire was used as a counter electrode and Ag/AgCl was used as a reference electrode. All the electrochemical experiments were conducted in 1 M KNO_3 electrolyte.

3. Results and discussion

3.1. Structural and morphological properties

The XRD profiles of as-prepared graphene, NiFeCN and NiFeCN/graphene are shown in Fig. 1a. All the peaks of NiFeCN and NiFeCN/graphene can be indexed as the crystalline nickel iron cyanide hydrate $Ni_3(Fe(CN)_6)_2(H_2O)$ (JCPDS no. 82-2283) (Chen et al., 2009; Guadagno et al., 2015). According to Sherrer equation (Patterson, 1939), the crystallite size was calculated to be 31 and 23 nm for pure NiFeCN and NiFeCN/graphene, respectively. The graphene sheets in the NiFeCN/graphene served as the platform for the nickel precursor adsorption and prevented the agglomeration of the NiFeCN nanoparticles. The NiFeCN nanoparticles were anchored onto the surface of graphene sheets by strong electrostatic interactions between ionic charge of the NiFeCN and negative surface charge on the graphene sheets, or by van der Waals interactions between NiFeCN and graphene (Wang et al., 2010; Kamat, 2010). On the other hand, NiFeCN particles acted as the spacers to prevent the stacking of graphene
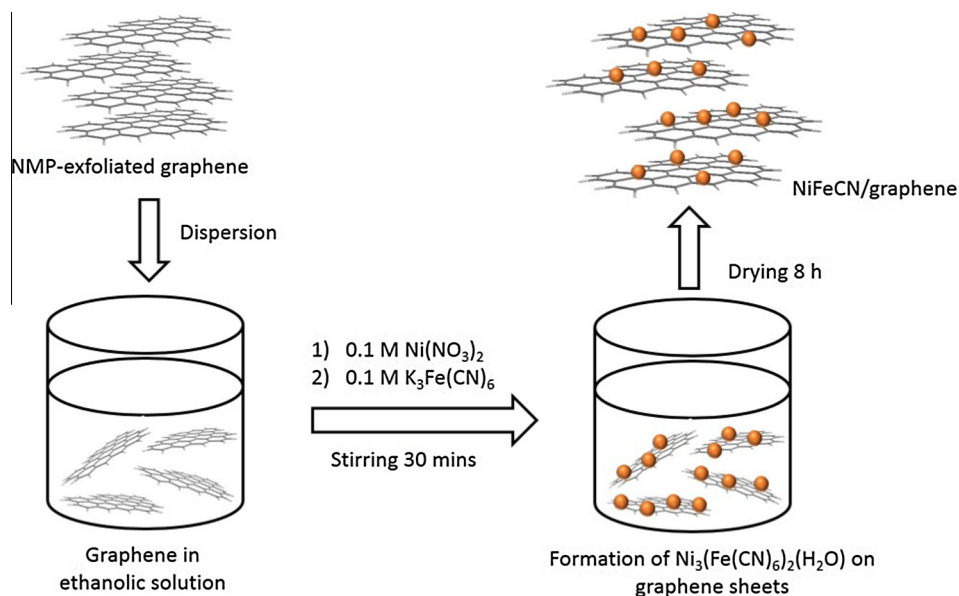
Scheme 1   The preparation of NiFeCN/graphene from NMP-exfoliated graphene.
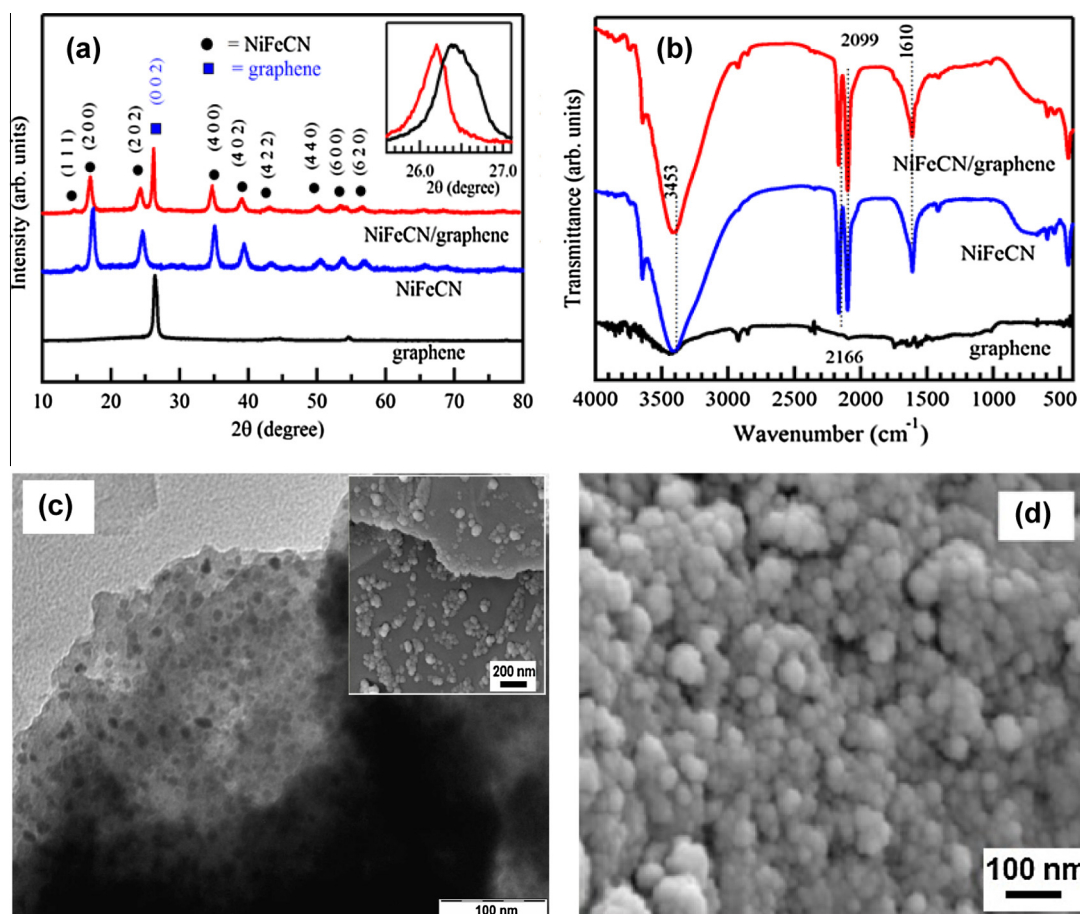

Figure 1   (a) XRD patterns, the inset shows the zoomed view of XRD (0 0 2) peaks; (b) FTIR spectra of graphene, NiFeCN and NiFeCN/graphene (11.24 wt% Fe); (c) representative TEM image of NiFeCN/graphene (11.24 wt% Fe), the inset shows the FESEM image; (d) representative FESEM image of NiFeCN.

sheets and the nanoparticles also caused the interlayer spacing increased from 0.337 nm to 0.340 nm, as indicated by the lower downshift of the (0 0 2) peak (from 26.43° to 26.19°) in NiFeCN/graphene (inset of Fig. 1a).

To further confirm the composition of NiFeCN/graphene, FTIR analysis was conducted on the samples (Fig. 1b). The hydrated nature of NiFeCN could be confirmed by the infrared absorption bands at 3453 and 1610 cm^{-1}, which could be assigned to the vibrations of the adsorbed water molecules (O─H) (Ng and Mintova, 2011). Strong bands at 2166 and 2099 cm^{-1} correspond to the C≡N group of Fe^{3+}-CN and of Fe^{2+}-CN, respectively (Cumba et al., 2012). The oxygen-related absorption peaks remained insignificant for graphene and revealed that the NMP-exfoliated graphene was unoxidized. The morphology of NiFeCN and NiFeCN/graphene were investigated by FESEM and TEM, respectively. From TEM analysis in Fig. 1c, it can be seen that the NiFeCN particles of ca. 20 nm in size were homogeneously grown on the surface of graphene sheets, which is in agreement with the XRD analysis. However, in the absence of graphene sheets, the NiFeCN particles (Fig. 1d) spontaneously agglomerated and formed large particles in the size of hundreds of nanometers. It suggests that the presence of graphene sheets plays an essential role in the dispersion of fine NiFeCN particles. EDX analysis showed that the Fe loading in NiFeCN/graphene was 11.24 wt% (see Table S1, Supporting Information).

3.2. Electrochemical performance

Cyclic voltammetry (CV), galvanostatic charge/discharge (CDC) and electrochemical impedance spectroscopy (EIS) were used to evaluate the electrochemical performance of as-prepared graphene, NiFeCN and NiFeCN/graphene electrodes. Fig. 2a shows the CV curves of as-prepared graphene, NiFeCN, and NiFeCN/graphene (11.24 wt% Fe) electrodes at 25 mV s^{-1} from 0 to 1 V, which were measured in 1 M KNO_3. The graphene electrode exhibited rectangular shape CV curve, an indicative of good double layer capacitance with rapid charge propagation. In contrast to graphene, NiFeCN electrode showed reversible redox peaks at the potential of ca. 0.5/0.4 V (Oxidation/Reduction). NiFeCN has tunnel structures due to the large asymmetric cyanide ions and this open space could accommodate ions insertion/desertion. Previous study reported that the NiFeCN showed electrochemical activity at low-spin iron ion redox center only and the nickel atom would remain at valence state (II) (Zamponi et al., 2003). Therefore, the redox peaks observed on NiFeCN electrode could be associated with the iron (II/III) couple coordinated by cyanide groups, which can be ascribed to the following reaction:

$$Ni^{II}_{1.5}[Fe^{III}(CN)_6] + K^+ + e^- \leftrightarrows KNi^{II}_{1.5}[Fe^{II}(CN)_6]$$
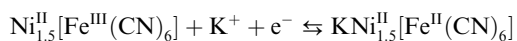
For *in situ* growth of NiFeCN on graphene sheets, the NiFeCN/graphene electrode showed dramatic increase in the redox current, which could be related to the increase in electroactive surface area (S_A). It is supported by the S_A calculation by Randles–Sevcik equation (Zamponi et al., 2003) that showed the S_A of NiFeCN/graphene electrode is ca. 36 times higher than that of NiFeCN electrode (see Supporting Information for calculation). The findings are in agreement with the FESEM observation where NiFeCN particles were

homogeneously grown on the graphene sheets, exposing more surface area for the redox reaction. However, the electron transfer was sluggish on the NiFeCN/graphene electrode, as seen from the large redox peak separation ($E_Δ$) on NiFeCN/graphene CV curve. Fig. 2b shows good linear relationship between peak current and square root of the scan rate for both NiFeCN and NiFeCN/graphene electrodes, indicating the redox reaction kinetics on both electrodes were controlled by the diffusion process of the potassium ions in the solution.

The ability of NiFeCN/graphene to be utilized as supercapacitors electrode was evaluated by galvanostatic CDC. NiFeCN/graphene (11.24 wt% Fe) showed the highest discharge time among all electrodes (Fig. 2c), indicating higher capacitive storage in this electrode. Moreover, it displayed two variation ranges in the charge and discharge curves, where linear variation (ca. 0–0.4 V; ca. 0.6–1.0 V) corresponds to the double layer capacitance and slope variation (ca. 0.4–0.6 V) corresponds to the pseudocapacitance. The specific capacitance (C_{sp}) values were calculated from the slope of the discharge curve using the equation reported elsewhere (Chen et al., 2009) and they are summarized in Fig. 2d. The highest specific capacitance (C_{sp}) attained on NiFeCN, graphene and NiFeCN/graphene electrodes was 18, 52 and 113.5 F g^{-1}, respectively at 0.25 A g^{-1}. It is interesting to note that the C_{sp} attained on NiFeCN/graphene electrode was 2 times higher than that of graphene electrode and 6 times higher than that of NiFeCN electrode. The findings imply that the *in situ* growth of NiFeCN on graphene sheets could synergistically enhance the double layer capacitance and pseudocapacitance effects, by preventing the graphene sheets from stacking and growing the NiFeCN particles homogeneously on the graphene sheets for higher S_A, as illustrated in Scheme 2. It is important for the *in situ* growth of NiFeCN on the graphene sheets as the electrode made from mixture of pure NiFeCN and pure graphene (by manual mixing) showed lower C_{sp} as compared to that of NiFeCN/graphene electrode (see Fig. S2, Supporting Information).

Since the redox-active Fe center in NiFeCN is responsible for the pseudocapacitance effect, it is crucial to study the effect of redox-active Fe loading on the specific capacitance enhancement, and NiFeCN/graphene electrodes with different Fe loadings of 2.97, 5.25, 7.43, 11.24 and 13.74 wt% (from EDX analysis) were prepared. Fig. 2e shows the CDC curves of NiFeCN/graphene electrodes with different Fe loadings, measured in 1 M KNO_3 at a current density of 0.25 A g^{-1}. As the Fe content increased, it could be seen that the discharge curves changed from linear variation to slope variation, implying that the predominant capacitive behavior was changed from EDLC to pseudocapacitive. The specific capacitance contribution from graphene and NiFeCN at different Fe loadings was carefully analyzed (Fig. 2f). The total C_{sp} showed monotonic increment with increasing Fe content and it is interesting to note that all C_{sp} values were much higher than the calculated capacitance $\left[C_{sp}^{cal} = C_{sp}^{NiFeCN} \times \frac{wt\%Fe}{20.7\%} + C_{sp}^{graphene} \times \left(1 - \frac{wt\%Fe}{20.7\%}\right)\right]$. The enhanced C_{sp} displayed the synergetic effect of graphene and NiFeCN in improving the electrochemical performance of NiFeCN/graphene electrode. The maximum C_{sp} enhancement was achieved at 11.24 wt% of Fe loading on graphene sheets. It could be attributed to the higher loading of NiFeCN particles that were evenly distributed on the graphene sheets, therefore producing more pseudocapacitive effect. At 13.74 wt% Fe
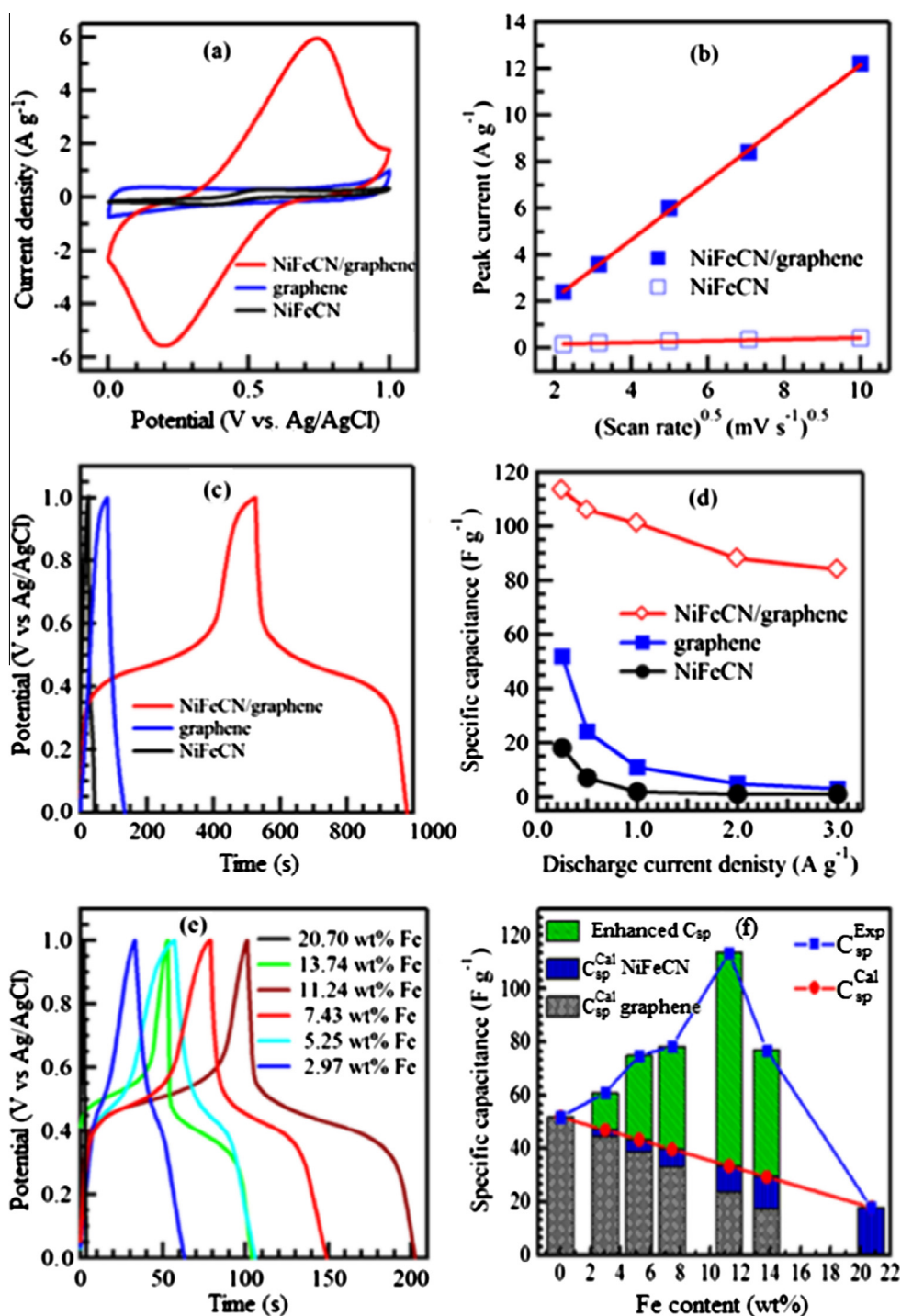
Figure 2 (a) CV curves at 25 mV s^{-1}; (b) anodic peak currents as a function of square root of scan rate; (c) CDC at 0.25 A g^{-1}; (d) specific capacitance as a function of current density; (e) CDC with different Fe loadings at 0.25 A g^{-1} and (f) calculated and experimental specific capacitance as a function of Fe loadings in NiFeCN/graphene.

loading, the C_{sp} enhancement was reduced, probably associated with the saturation of NiFeCN particles that lead to agglomeration on the graphene sheets. Fig. 3a shows the electrochemical stability of NiFeCN/graphene (11.24 wt% Fe) electrode for 10,000 CDC cycles at 2 A g^{-1}. It could be seen that the NiFeCN/graphene electrode exhibited high electrochemical stability by retaining 87% of the capacitance at the end of 10,000 CDC cycles. Such high electrochemical stability was

comparable to the stability of double layer capacitance material (graphene) at 96%. In addition, the electrochemical stability was also significantly enhanced as compared to that of pseudocapacitance material (NiFeCN) at 60%. On the other hand, the CDC curve of NiFeCN/graphene shows little variation after 10,000 cycles, as depicted in the insets of Fig. 3a. Nyquist plots (Fig. 3b) show that the equivalent series resistance (ESR) was 1.95, 1.50 and 0.65 Ω for graphene, NiFeCN and
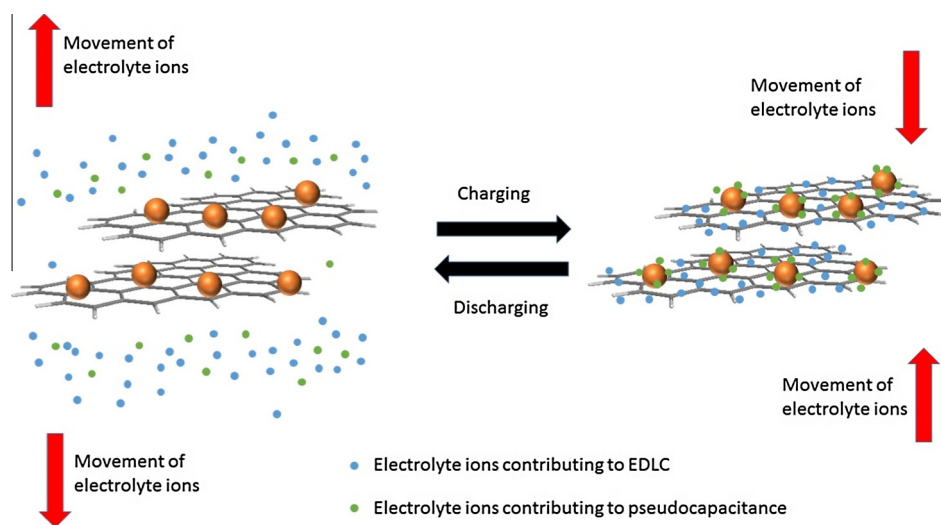
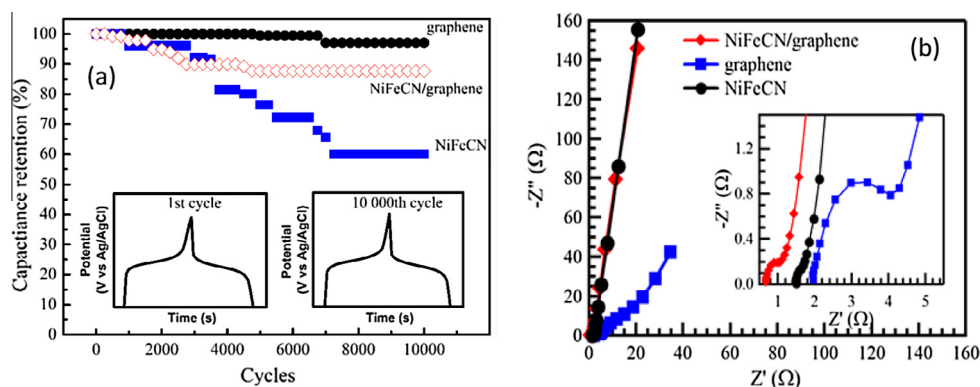**Scheme 2**   The charge and discharge mechanism of NiFeCN/graphene.

Figure 3   (a) Stability test of NiFeCN/graphene (11.24 wt% Fe), graphene and NiFeCN electrodes at 2 A g^{-1}, the insets show the CDC curves of NiFeCN/graphene (11.24 wt% Fe) at 1st and 10,000th cycles; (b) impedance spectra of graphene, NiFeCN and NiFeCN/graphene (11.24 wt% Fe).

NiFeCN/graphene (11.24 wt% Fe), respectively. Lower ESR value was shown by NiFeCN/graphene electrode implying that it could be used in the high-power supercapacitor as the power density, $P = \frac{V^2}{4 \times ESR}$. However, the charge transfer resistance (R_{CT}) for NiFeCN/graphene electrode was higher than that of NiFeCN electrode, similar as CV findings that showed sluggish electron transfer. The equivalent circuit fitting for NiFeCN/graphene is shown in Fig. S3 (Supporting Information).

4. Conclusions

Redox-active NiFeCN particles were successfully grown on the NMP-exfoliated graphene sheets by using facile co-precipitation method. 20 nm NiFeCN particles were homogeneously distributed on graphene sheets and they acted as the spacers between neighboring graphene sheets. The NiFeCN/graphene exhibited specific capacitance of 113.5 F g^{-1}, which was 2 times higher than the graphene (52 F g^{-1}) and 6 times higher than the NiFeCN (18 F g^{-1}). Moreover, the total specific capacitance values for NiFeCN/graphene electrode were higher than the simple sum of specific capacitance of graphene and NiFeCN in their relative weight ratios. The specific capacitance enhancement of NiFeCN/graphene could be associated with the

positive synergistic effect of graphene and NiFeCN due to the well-separated graphene sheets, increased electroactive surface area of NiFeCN, and the high conductivity network of fine NiFeCN particles. In addition, NiFeCN/graphene exhibited good electrochemical cycling stability (87% after 10,000 cycles). Considering the full utilization of the advantages of graphene and NiFeCN, the *in situ* growth of NiFeCN onto graphene sheets could provide a facile approach to modify NMP-exfoliated graphene for the energy storage applications.

Appendix A. Supplementary material

Supplementary data associated with this article can be found, in the online version, at http://dx.doi.org/10.1016/j.arabjc.2016.02.006.

References

Ali, G.A.M., Fouad, O.A., Makhlouf, S.A., Chong, K.F., 2014a. Co_3O_4/SiO_2 nanocomposites for supercapacitor application. J. Solid State Electrochem. 18, 2505–2512.

Ali, G.A.M., Makhlouf, S.A., Yusoff, M.M., Chong, K.F., 2015. Structural and electrochemical characteristics of graphene nanosheets as supercapacitor electrodes. Rev. Adv. Mater. Sci. 41, 35–43.

Ali, G.A.M., Manaf, S.A.B.A., Kumar, A., Chong, K.F., Hegde, G., 2014b. High performance supercapacitor using catalysis free porous carbon nanoparticles. J. Phys. D: Appl. Phys. 47, 495307–495313.

Ali, G.A.M., Tan, L.L., Jose, R., Yusoff, M.M., Chong, K.F., 2014c. Electrochemical performance studies of mno2 nanoflowers recovered from spent battery. Mater. Res. Bull. 60, 5–9.

Arslan, A., Hür, E., 2012. Supercapacitor applications of polyaniline and poly (n-methylaniline) coated pencil graphite electrode. Int. J. Electrochem. Sci. 7, 12558–12572.

Borgohain, R., Yang, J., Selegue, J.P., Kim, D.Y., 2014. Controlled synthesis, efficient purification, and electrochemical characterization of arc-discharge carbon nano-onions. Carbon 66, 272–284.

Cao, X., Yin, Z., Zhang, H., 2014. Three-dimensional graphene materials: preparation, structures and application in supercapacitors. Energy Environ. Sci. 7, 1850–1865.

Chen, J., Huang, K., Liu, S., Hu, X., 2009. Electrochemical supercapacitor behavior of $Ni_3(Fe(CN)_6)_2(H_2O)$ nanoparticles. J. Power Sources 186, 565–569.

Chen, Q., Zhao, Y., Huang, X., Chen, N., Qu, L., 2015. Three-dimensional graphitic carbon nitride functionalized graphene-based high performance supercapacitors. J. Mater. Chem. A 3, 6761–6766.

Cumba, L.R., Bicalho, U.d.O., Silvestrini, D.R., Carmo, D.R.d., 2012. Preparation and voltammetric study of a composite titanium phosphate/nickel hexacyanoferrate and its application in dipyrone determination. Int. J. Chem. 4, 66–78.

Gao, L., Guest, J.R., Guisinger, N.P., 2010. Epitaxial graphene on Cu (111). Nano Lett. 10, 3512–3516.

Guadagno, L., Sarno, M., Vietri, U., Raimondo, M., Cirillo, C., Ciambelli, P., 2015. Graphene-based structural adhesive to enhance adhesion performance. RSC Adv. 5, 27874–27886.

Hernandez, Y., Nicolosi, V., Lotya, M., Blighe, F.M., Sun, Z., De, S., McGovern, I.T., Holland, B., Byrne, M., Gun'Ko, Y.K., Boland, J.J., Niraj, P., Duesberg, G., Krishnamurthy, S., Goodhue, R., Hutchison, J., Scardaci, V., Ferrari, A.C., Coleman, J.N., 2008. High-yield production of graphene by liquid-phase exfoliation of graphite. Nat. Nanotechnol. 3, 563–568.

Kamat, P.V., 2010. Graphene based nanoarchitectures. Anchoring semiconductor and metal nanoparticles on a 2-dimensional carbon support. J. Phys. Chem. Lett. 1, 520–527.

Krishnamoorthy, K., Kim, S.J., 2015. Mechanomechanical preparation of graphene nanosheets and their supercapacitor applications. J. Ing. Eng. Chem. 32, 39–43.

Krishnamoorthy, K., Thangavel, S., Veetil, J.C., Raju, N., Venugopal, G., Kim, S.J., 2015. Graphdiyne nanostructures as a new electrode material for electrochemical supercapacitors. Int. J. Hydrogen Energy. http://dx.doi.org/10.1016/j.ijhydene.2015.10.118.

Liu, C.G., Yu, Z.N., Neff, D., Zhamu, A., Jang, B.Z., 2010. Graphene-based supercapacitor with an ultrahigh energy density. Nano Lett. 10, 4863–4868.

Liu, J., Zhang, L., Wu, H.B., Lin, J., Shen, Z., Lou, X.W.D., 2014. High-performance flexible asymmetric supercapacitors based on a new graphene foam/carbon nanotube hybrid film. Energy Environ. Sci. 7, 3709–3719.

Liu, W., Li, H., Xu, C., Khatami, Y., Banerjee, K., 2011. Synthesis of high-quality monolayer and bilayer graphene on copper using chemical vapor deposition. Carbon 49, 4122–4130.

Liu, X.B., Wen, N., Wang, X.L., Zheng, Y.Y., 2015. Layer-by-layer self-assembled graphene multilayer films via covalent bonds for supercapacitor electrodes. Nanomater. Nanotechnol. 5, 1–7.

Ng, E.-P., Mintova, S., 2011. Quantitative moisture measurements in lubricating oils by FTIR spectroscopy combined with solvent extraction approach. Microchem. J. 98, 177–185.

Pang, H., Zhang, Y., Cheng, T., Lai, W.Y., Huang, W., 2015a. Uniform manganese hexacyanoferrate hydrate nanocubes featuring superior performance for low cost supercapacitors and nonenzymatic electrochemical sensors. Nanoscale 7, 16012–16019.

Pang, H., Zhang, Y., Lai, W.Y., Hu, Z., Huang, N., 2015b. Lamellar $K_2CO_3(P_2O_7)\cdot 2H_2O$ nanocrystal whiskers: high-performance flexible all-solid-state asymmetric micro-supercapacitors via inkjet printing. Nano Energy 15, 303–312.

Patterson, A., 1939. The Scherrer formula for X-ray particle size determination. Phys. Rev. 56, 978–982.

Ramya, R., Sivasubramanian, R., Sangaranarayanan, M.V., 2013. Conducting polymers-based electrochemical supercapacitors-progress and prospects. Electrochim. Acta 101, 109–129.

Sun, L., Fugetsu, B., 2013. Mass production of graphene oxide from expanded graphite. Mater. Lett. 109, 207–210.

Teo, E.Y.L., Lim, H.N., Jose, R., Chong, K.F., 2015. Aminopyrene functionalized reduced graphene oxide as a supercapacitor electrode. RSC Adv. 5, 38111–38116.

Teo, E.Y.L., Zaid, R.M., Ling, T.L., Chong, K.F., 2012. Facile corrosion protection coating from graphene. Int. J. Chem. Eng. Appl. 3, 453–455.

Vidhyadharan, B., Zain, N.K.M., Misnon, I.I., Aziz, R.A., Ismail, J., Yusoff, M.M., Jose, R., 2014. High performance supercapacitor electrodes from electrospun nickel oxide nanowires. J. Alloys Compd. 610, 143–150.

Wang, H., Robinson, J.T., Diankov, G., Dai, H., 2010. Nanocrystal growth on graphene with various degrees of oxidation. J. Am. Chem. Soc. 132, 3270–3271.

Wang, L., Ye, Y., Lu, X., Wen, Z., Li, Z., Hou, H., Song, Y., 2013. Hierarchical nanocomposites of polyaniline nanowire arrays on reduced graphene oxide sheets for supercapacitors. Sci. Rep. 3, 3568–3577.

Wang, Y., Shi, Z.Q., Huang, Y., Ma, Y.F., Wang, C.Y., Chen, M.M., Chen, Y.S., 2009. Supercapacitor devices based on graphene materials. J. Phys. Chem. C 113, 13103–13107.

Wen, P., Gong, P., Mi, Y., Wang, J., Yang, S., 2014. Scalable fabrication of high quality graphene by exfoliation of edge sulfonated graphite for supercapacitor application. RSC Adv. 4, 35914–35918.

Wu, Z.S., Wang, D.W., Ren, W., Zhao, J., Zhou, G., Li, F., Cheng, H.M., 2010. Anchoring hydrous RuO_2 on graphene sheets for high-performance electrochemical capacitors. Adv. Funct. Mater. 20, 3595–3602.

Zaid, R.M., Chong, F.C., Teo, E.Y.L., Ng, E.-P., Chong, K.F., 2015. Reduction of graphene oxide nanosheets by natural beta carotene and its potential use as supercapacitor electrode. Arab. J. Chem. 8, 560–569.

Zamponi, S., Berrettoni, M., Kulesza, P.J., Miecznikowski, K., Malik, M.A., Makowski, O., Marassi, R., 2003. Influence of experimental conditions on electrochemical behavior of prussian blue type nickel hexacyanoferrate film. Electrochim. Acta 48, 4261–4269.

Zhang, Y.Z., Wang, Y., Cheng, T., Lai, W.Y., Hu, Z., Pang, H., Huang, W., 2015. Flexible supercapacitors based on paper substrates: a new paradigm for low-cost energy storage. Chem. Soc. Rev. 44, 5181–5199.